How Cu I and Na I Interact with Faujasite Zeolite? A Theoretical Investigation

Hugo Petitjean, Christine Lepetit, Zalfa Nour, Romuald Poteau, Iker Del rosal, Dorothée Berthomieu

How Cu^{I} and Na^{I} interact with faujasite zeolite: a theoretical investigation

Hugo Petitjean,[1] Christine Lepetit,[2] Zalfa Nour,[3] Romuald Poteau,[4] Iker del Rosal,[4] Dorothée Berthomieu[1]*

[1]ICGM, Univ Montpellier, CNRS, ENSCM, Montpellier, France

[2]LCC-CNRS, Université de Toulouse, CNRS, UPS, Toulouse – France

[3]Lebanese University, Faculty of Science, branch 3 – Lebanon

[4]LPCNO, UMR 5215 CNRS-INSA-UPS, 135 avenue de Rangueil 31077 Toulouse Cedex 4 – France.

dorothee.berthomieu@enscm.fr

ORCID

D. Berthomieu: 0000-0002-3818-105X

ABSTRACT:

Zeolite materials have complex structures that can be determined by X-Ray diffraction but characterizing the non-periodic defects, the distribution of the aluminum atoms and the position of the exchanged cations remain a challenge. It was shown that quantum chemistry methods (QM) are well suited to predict the structure, even with low symmetry. Here, QM were used to determine the location and coordination of Na^I and Cu^I cations in Si-rich faujasites of Y-type (with moderate Si/Al ratio) and Al-rich faujasites of X-type (Si/Al = 1). Focusing on the first shell of the metal site, we used QM analysis tools to study the various distortions induced by the presence of Al in the rings of faujasites. Such microscopic data was not accessible using experimental XRD methods. In contrast, using the present theoretical approach, it was possible to predict the absence of symmetry at the atomic level, and that sites I were not occupied by Na^I nor by Cu^I cations, even for Al-rich faujasites of X-type. The infrared CO probe was used to analyze the interaction of both Na^I and Cu^I with the zeolite framework. Single CO adsorption on Na^I and Cu^I *via* the carbon atom showed that the calculated ν_{CO} stretching frequency bands are mainly upshifted in comparison with isolated CO. The ν_{CO} stretching frequency range was predicted to be larger for Cu^I than for Na^I and the bandwidth would be affected by different Al distributions in the 6-membered rings (6MR): the more Al atoms in the 6MR, the larger the bandwidth. To capture insights of metal bonding picture with its neighbors, we performed natural bond orbital analysis (NBO) combined with quantum theory of atoms in molecules and electron localization function topological analyses (QTAIM and ELF methods, respectively). While it is generally reported that Na cations provide electrostatic interactions with zeolite materials, Cu cations is often assumed to favor covalent interactions. The upshifting of the calculated ν_{CO} stretching frequency and our topological analyses rather indicated that the interactions of Na^I and Cu^I with the oxygen atoms of the hosted zeolite

were mainly ionic with a weak covalent character in the case Cu^I. The adsorption of CO on Na^I proceeds *via* an ionic Na---C interaction, while for Cu^I, the Cu---CO bond was calculated to be dative with a strong polar character. Whatever the Lewis metal cation, Cu^I or Na^I, the present topological analyses predict that their interactions with the O atoms of the zeolite were ionic.

Corresponding Author

Key Words: zeolites, faujasites, adsorption, CO, metals, DFT, periodic, enthalpies, vibrations, topology analyses

INTRODUCTION:

Zeolites are generally classified among the most efficient porous materials for adsorption-based applications, industrially used for the selective adsorption of gases. Structurally, zeolites are aluminosilicates built from tetrahedral units (labeled T) made of four oxygen atoms bonded to silicon (SiO_4) or aluminum (AlO_4).[1-2] Each silicon atom substituted by an aluminum atom generates a negative net charge in the structure that can be balanced by the addition of protons and/or cations. There is a large variety of zeolitic structures and their frameworks have different channels, cage shapes and sizes. The silicon/aluminum ratio and the cation types are controlled during synthesis. The Si/Al ratio and the nature of the cations (alkali, transition metal ions etc….) are essential parameters as they influence the adsorption, separation, diffusion and catalytic properties. Faujasite (FAU) zeolites are tridimensional aluminosilicate materials for which the Si/Al ratio and the distribution of the extra-framework cations can be controlled during the synthesis. FAU X-type zeolites usually have Si/Al ratio in the range of 1 while FAU Y-type zeolites have Si/Al ratio larger than 1.[3] The FAU framework consists of rings with 4 and 6 tetrahedra (T) organized in tridimensional structures of three types: supercages, with a diameter in the range of 13Å (Figure 1), sodalite cage units and prisms.[4]

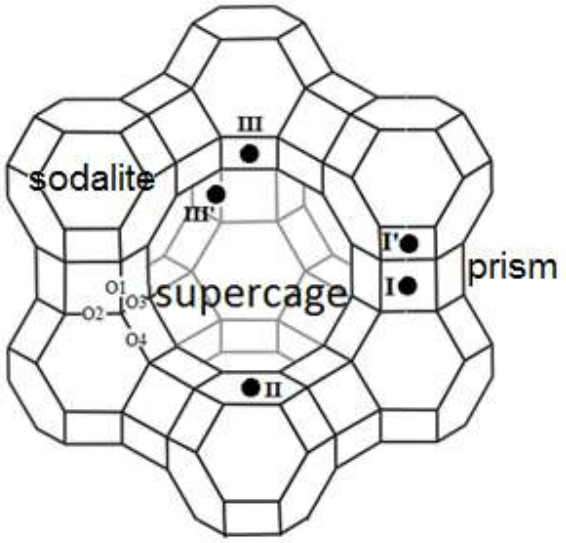

Figure 1. Faujasite unit cell and crystallographic positions in the supercage, sodalite and in the prism cages. Based on a cubic symetry, four different O types were determined: i/ O_1 sharing two four membered rings of the hexagonal prism cage, ii/O_2 connecting a four membered ring of an hexagonal prism and a six-membered ring of a sodalite cage, iii/O_3 are oxygen atoms shared both by four membered rings, one from an hexagonal prism and one from a sodalite cage, iv/ O_4 sharing a four membered ring and a six membered ring of a sodalite cage.

Faujasites exchanged with copper or sodium provide a unique model to address debated questions on the location and the coordination properties of extraframework metal sites in zeolites. These materials are frequently used for very efficient catalytic and adsorption properties.[3] Na^I and Cu^I are classified as Lewis acid cations, and they are expected to have opposite electronic properties in their interactions with the framework oxygen atoms and the adsorbed molecules. The electronic properties of the extraframework cations are crucial, of course, for the applications of the zeolites but also for their characterization. Indeed, the zeolite crystallographic structure can be characterized with X-Ray Diffraction (XRD) only in an incomplete manner because XRD cannot

localize the aluminum tetraedra and the associated extraframework cations that are disorderedly distributed in the structure. To get deeper insights on the metal sites, chemists often probe the extraframework cations through their electronic properties by adsorbing molecules and investigating associated responses in spectroscopy or thermal analysis.

Carbon monoxide is one of these probe-molecules. It is involved in many chemical and industrial processes and its removal is of great importance to reduce detrimental environmental and climate impacts. Zeolites are used either as membranes for the removal of carbon monoxide and for the purification of gas mixtures. Carbon monoxide is also widely used as a probe molecule to characterize Lewis and Brønsted acid sites from zeolites. When adsorbed on alkali and transition metal cations such as sodium or copper cation, it yields strong bands in the easily accessible medium infrared (IR) domain corresponding to the CO stretching mode.[5] The ν_{CO} stretching frequency values depend on the strength and the nature of the bond formed with the metal cation. This is a marker used to characterize the nature and the location of the cations in the zeolite framework. In FAU-type zeolites, CO mainly adsorbs on cations of the largest cages (e.g. the supercage).[6] Because it remains difficult to relate the frequency value of the ν_{CO} bands to the crystallographic positions of the cations in the zeolite framework, the combination of experimental and theoretical approaches is required to characterize the zeolite structures with CO adsorption followed by FTIR.

Theoretical approaches of adsorption in porous materials use molecular dynamic simulations or first principle calculations depending on the properties under investigation. While molecular dynamic simulations with classical force fields provide information on large systems under defined pressure and temperature values of adsorbents, it is less reliable for the description of transition

metal ions. In contrast, quantum chemistry methods provide accurate geometries and correctly describe the bonding with transition metal ions such as copper.

The aim of the present study is to predict the coordination modes of metal-exchanged faujasites for mononuclear metal species, to investigate the origin of the ν_{CO} stretching frequency shift with adsorption, and to characterize M---O_{FAU} and M---CO interactions using state of the art chemical bonding analysis methods.[7-8] It is a theoretical study at the DFT level, including comparison with experimental results from literature. It focuses on a series of faujasite zeolites (Figure 1), with Si/Al ratio of 1 and ~2.4 and exchanged with Na^I and Cu^I, two types of metal cations (alkali and transition metal). These zeolites with two different Si/Al ratio were chosen to be compared with experimental crystallographic structure analyses. As the Al distributions in the framework of zeolites unit cell are not known experimentally,[9-11] we modelled FAU structures by varying the Al distribution in the framework and in particular in the six-membered rings. This variety of models will allow the bonding of Cu^I and Na^I with CO to be characterized in zeolite porous materials with various adsorption configurations: single or multiple adsorptions on a same centre or with a same CO molecule linked to one or two centres.[12]

The type of bonding involving extraframework metal cations will be determined in their interactions with the nearby framework O atoms of the zeolite and with the CO probe, using three computational analysis methods: Natural Bond Orbital (NBO),[13] Quantum Theory of Atoms in Molecules (QTAIM)[14] and Electron Localization Function (ELF)[15] topological analyses. Based on these approaches, metal ions will be classified depending on their ability to form ionic or dative covalent bonds with ligands.

The structures were optimized and the vibrational frequencies were computed at the GGA and B3LYP levels in periodic conditions to account for long-range interactions and confinement effect

in the zeolites. To reduce the computational efforts demanded, cluster models[16] were also considered in order to take a bonding picture from NBO analysis, QTAIM and ELF topological analyses.

The final discussion addresses the factors influencing the frequency shift of the ν_{CO} value upon adsorption of CO in the Cu^{I}- and Na^{I}-exchanged faujasites. Although several reports are discussing metal-ligand interactions in terms of the relative contributions of electrostatic and electron-sharing (covalent) interactions,[12] it is still unclear why the experimental ν_{CO} value of CO adsorbed on Cu^{I}-exchanged zeolites is upshifted (blueshifted) in comparison to isolated CO and to copper carbonyl derivatives.[17-18] It is generally explained using frontier molecular orbital theory that adsorption of CO on Cu^{I} sites provided strong σ-bonds involving the HOMO 5σ bond from CO to the LUMO of the metal cation and π-bonds resulting from π back-donation from metal cations to the antibonding 2π* of CO.[5] Present analyses contribute to determine the nature of the interaction between alkali or transition metal cations with oxygen atoms of the zeolite framework and with CO. While the nature of Lewis acid interaction with the zeolite has long been a recurrent question from chemists eager to classify the metal bond interaction types with surfaces, the present study aims at characterizing metal cation interactions in zeolite materials, in particular with their surrounding framework O atoms.

Theoretical methods.

Models

To model the faujasite unit cell containing 192 T sites with a general formula for the hydrated Na-exchanged faujasite $Na_{58}Al_{58}Si_{134}O_{384}.240H_2O$ and a cubic Fd$\underline{3}$m symmetry,[19] we built simplified periodic structures containing 48 T sites with a (face-centered cubic) rhombohedra

symmetry, as previously reported,[20] with the cell parameters: *a*) 17.9103 Å, *b*) 18.0444 Å, *c*) 17.72 Å, α) 59.7463°, β) 61.1221°, γ) 59.4924°, and a volume of 4058.55 $Å^3$. The cell parameters were fixed to these values during geometry optimizations while all the atoms were allowed to relax in order to minimize both the forces on the atoms and the pressure on the unit cell. This choice was made in order to compare the properties of structures. In the primitive unit cell model, the number of the five most frequently occupied crystallographic sites (Sites I, I', II, III and III' in Figure 1) by metal cations is smaller than in the large cubic unit cell. We considered two different Si/Al ratios (1 and ~2.4) and two different metals (Na and Cu). The Si/Al ratio is 1 in (Al_{24} M_{24} O_{96} Si_{24} with M = metal) and ~2.4 in (Al_{14} $M_{14}O_{96}$ Si_{34}, M = metal). These structures obey the Loewenstein rule (i.e. no Al-O-Al sequence).[21]

The models of FAU Y and X zeolites were built and optimized with one exchanged metallic cation per aluminum and 3 different Na/Cu ratios: only Na^I , 23 Na^I for 1 Cu^I, and only Cu^I. For the FAU Y-type zeolite structures, with Si/Al ratio of ~2.4 and the same distribution of framework aluminum ions, geometry optimizations converged toward two different cation distributions: A (3 SI' 1 SIII, 2 SIII′, and 8 SII) and B (6 SI' and 8 SII). To explore the influence of the aluminum content in the 6MR, we also built a model with one Al-O-Si-O-Al-O-Si-O-Al sequence in a 6MR (converging to a B geometry), which was not present in the other Y models. For the FAU X-type zeolites with a Si/Al ratio of 1, geometry optimizations converged to a cation distribution labelled C (8 SI', 8 SIII' and 8 SII).

In the model containing 8 CO, the CO positions were chosen to be in proximity of each metal cation and with the C atom closer to the metal cation than the O atom. This model was chosen to have one layer of CO adsorbed on one metal cation (according to a type I isotherm model). In the model containing 12 CO, different types of adsorptions were considered (O end adsorption, dual

M…C=O…M adsorption and polyadsorptions). In the initial structures, CO was not adsorbed in the sodalite neither in the prism cages because experimental results indicate that the CO molecules are too large to enter in the sodalite or in the prism cages.[6] With CO adsorbed in the zeolite structure, present geometry optimizations may converge to cation distributions different from what was obtained without CO (Table 3, Tables S2-S4). To investigate the potential energy surface of the zeolite structures containing CO, we calculated Ab Initio Molecular dynamics on periodic structures. Because the periodic models are large, and have many degrees of freedom, standard AIMDs were performed (in the canonical ensemble, during few nanoseconds, a time step of 0.5 fs and at 200 K) followed with geometry optimizations.

For ELF and QTAIM topological investigations, we only used the smallest clusters (6 T), easier to be handled. For Natural Bond Orbital analyses, we used both large and small clusters. They were cut from a periodic structure as previously described.[22]

Quantum chemical calculations

Two different DFT methods were mainly used: the PBE exchange-correlation functional[23-26] and the B3LYP hybrid functional.[24] When included, dispersion was calculated using the empirical dispersion term D*.[27-28]

The projector augmented wave approximation (PAW) of Bloechl[29-30] and a kinetic energy cutoff of 600 eV were used. These calculations were performed using the vasp.5.2.2 and vasp.5.3.5 version programs.[31-34]

PBE-D*/BS1 and B3LYP-D*/BS1 calculations[24, 27-28] were performed with the massive parallel version of the periodic ab-initio Crystal 2014 code.[35] The Crystal code was used because it is very fast for B3LYP-D*/BS1 calculations and enables to bridge the gap between periodic models using PAW and cluster models using gaussian-type atom-centered all-electron basis sets. For the

calculations using periodic structures and gaussian-type atom-centered all-electron basis sets (with the Crystal 2014 code), the unit cell parameters were set to the parameters reported above and kept fixed during geometry optimizations while all the atoms were allowed to relax. For the periodic calculations using PBE-D*/BS1 and B3LYP-D*/BS1 methods, the wave function was developed on gaussian-type atom-centered all-electron basis sets including 2810 basis functions for $(OC)_{12}Al_{14}Na_{14}O_{96}Si_{34}$ and 2894 for $(OC)_8Al_{14}Cu_{14}O_{96}Si_{34}$, respectively. SCF convergence was set to 10^{-7} Hartree for the energy during geometry optimization. The shrinking factor of the reciprocal space net was 2. Large double or triple zeta basis sets were used for Al,[36] Si,[37] Na,[38] O[39], Cu[40] and C.[39]

The cluster models were calculated with the Gaussian program[41] using the hybrid B3LYP method, and the 6-31G(d) basis set for the large 42 T cluster model[20] and the 6-311G(d,p) basis set for the 6 T.[22] These methods were labelled B3LYP/6-31G(d) and B3LYP/6-311G(d,p) respectively.

Harmonic vibrations of the ν_{CO} modes were estimated using a finite-difference approximation, consistently with previous studies.[20] Because previous calculations showed that the CO vibration involves only C and O atoms,[20, 22] only C and O were allowed to relax. ν_{CO} frequency values at the gamma point provide the displacement value of C and O with respect to their atomic coordinates in the optimized structures.

Frequency values for CO were calculated for the isolated CO in a periodic box.[20, 22] Molden[42] and moldraw[43] programs were used to read output files and to generate crystallographic structure files. The average bonds were calculated using the bond distances computed using the platon program.[44]

Natural Bond Orbital Analysis[7, 45-46] were performed using the NBO version implemented in the host Gaussian program.

Topological analyses. Electron Localization Function (ELF) topological analysis and Quantum Theory of Atoms in Molecules (QTAIM) analysis were performed with the TopMoD package[47] at the B3LYP/6-311G(d,p) level using 6 T cluster models only. QTAIM[14] analyses were also performed with the AIMAll software.[48] Topological methods are based on the analysis of the gradient field of a local function within the dynamic field theory and provide a partition of the molecular space into non-overlapping basins.

The topological analysis of the electron density $\rho(r)$, designed as the Quantum Theory of Atoms in Molecules (QTAIM) by R. Bader, yields atomic basins and QTAIM atomic charges.[14] It allows defining bond paths and bond critical points (BCPs). The nature of the chemical bond is characterized from various properties of the electron density at the BCPs, especially the sign of the Laplacian of the electron density and the values of the kinetic energy density ($\boldsymbol{G_{bcp}}$), of the potential energy density ($\boldsymbol{V_{bcp}}$) and of the energy density $\boldsymbol{H_{bcp}} = \boldsymbol{G_{bcp}} + \boldsymbol{V_{bcp}}$ following the Bianchi's[49] and Macchi's classification.[50] Negative and positive values for the Laplacian of the electron density at the BCP ($\boldsymbol{\Delta\rho_{bcp}}$) are assigned to « electron-shared » and « closed-shell » interactions, respectively.[14, 48] Bianchi *et al.*[49] distinguish three bonding regimes, depending on the value of the absolute ratio of the potential energy density to the kinetic energy density ($\boldsymbol{|V_{bcp}|/G_{bcp}}$). The intermediate bond regime ($1 < \boldsymbol{|V_{bcp}|/G_{bcp}} < 2$) lies between electron-shared covalent bonds ($\boldsymbol{|V_{bcp}|/G_{bcp}}$ greater than 2) and closed-shell ionic bonds or van der Waals interactions ($\boldsymbol{|V_{bcp}|/G_{bcp}}$ lower than 1) and includes dative bonds and ionic bonds of weak covalent character. The Macchi's classification[50] relies on the values of both local descriptors and

the delocalization index (DI) and offers a way to refine the bond characterization further. The covalence degree may be estimated from the latter and from $|\boldsymbol{H_{bcp}}|/\boldsymbol{\rho_{bcp}}$.[51]

The strength of the interaction may be estimated from the correlation scheme of Espinosa *et al.* [52-53] providing the corresponding positive interaction energy ($E_{int} = - ½ \mathbf{V_{bcp}}$), with E_{int} (kcal mol^{-1}) = -313.754 x $\mathbf{V_{bcp}}$ (au)).

The electron localization function (ELF) measures the excess of kinetic energy due to the Pauli repulsion.[15, 54] ELF values are confined between 0 and 1. ELF tends to a value of 1 in those regions where the electron localization is high (atomic shells, chemical bonds, and single electron or lone pairs) whereas it tends towards small values at the boundaries between these regions. The topological analysis of the ELF gradient field yields a partition of the molecular space into non-overlapping electronic domains, classified into core, valence bonding and nonbonding basins. These basins are in one-to-one correspondence to the core, lone or shared pairs of the Lewis model. A core basin contains a nucleus X (except a proton) and is designated as C(X). A valence basin lies between two or more core basins. Valence basins are further distinguished by their synaptic order, which is the number of core basins with which they share a common boundary. The monosynaptic basins denoted as V(X), correspond to lone pairs, whereas the di- and polysynaptic ones are related to bi- or multi-centric bonds, denoted as V(X1, X2, X3, ...). The average population of the basin is obtained by integration of the one-electron density over the basin volume. These populations do not take integral values and are about twice the topologically defined Lewis bond orders for bonding valence basins.

Results and discussion

Bare metal-exchanged faujasite structures

The faujasite zeolite presents various crystallographic sites. The most relevant sites for adsorption are indicated in Figure 1, along with their usual labellings.[4, 19] The crystallographic sites are occupied by metal cations in the vicinity of substituted Al atoms. We considered different Al distributions and different Al loadings (§ models in computational details) using the PBE functional and PAW method. The computed geometrical parameters were compared with experimental diffraction data (Tables 1, 2 and S2).

Table 1. Geometrical parameters (Å) of sodium- and copper-exchanged FAU Y-type zeolites: results from geometry optimization of A and B periodic models with PBE functional and PAW method, compared with experimental diffraction data.[55-58] Comparison of Geometrical Parameters between DFT calculations and experiments of sodium and copper-exchanged FAU Y-type zeolite. Two periodic models (labelled A and B) were optimized. Model B with the $Al_{14}Cu_{14}O_{96}Si_{34}$ formula contains one Al-O-Si-O-Al-O-Si-O-Al sequence but not model B with the $Al_{14}Na_{14}O_{96}Si_{34}$ formula. Geometry optimizations were performed using the PBE for exchange correlation and PAW method.

Method	**PBE**			**Experimental diffraction data**				
Label in the study or ref	A	B	B	[57]	[55]	[56]	[56]	[58]
Si/Al	~2.4	~2.4	~2.4	2.4	2.4	2	2	2.7
Formula or reference	$Al_{14}Na_{14}O_{96}Si_{34}$	$Al_{14}Na_{14}O_{96}Si_{34}$	$Al_{14}Cu_{14}O_{96}Si_{34}$	$Al_{56}Na_{56}O_{384}Si_{136}$	$Al_{57}Na_{57}O_{384}Si_{135}$	$Al_{64}Na_{62}O_{384}Si_{128}$	$Cu^{I}Y$	$Cu^{I}Y$
Occupied M (metal) site positions	I'(3)[a] III'(1)[a] III (2)[a]II (8)[a]	I'(6) [a] II (8)[a]	I'(6)[a] II (8)[a]	II' II	I, II, III	I_A', I_B', II′, II	I_A', I_B', II′, II	I* II* II
(Si/Al)-O Average	1.704	1.705	1.711	1.649	1.635	1.644	1.63	1.667
M(I)---O		-		2.718[b]	2.33[c]	2.689[b]	(I'_A) 2.22	

							(I'_B) 2.64 (I'_B) 1.93	
M(I')---O	2.278-3.013[d]	2.300-2.947[d]	2.078-3.172[d]	2.24-2.93[e]		2.246-2.941 [f]		(I*) 2.001
M(II)---O	2.353-2.844[d]	2.361-2.843[d]	2.045-2.992[d]	2.39-2.86[g]	3.10[h]-2.44[i]	2.38-2.865[j]	(II') 2.222	(II*) 2.033 (II) 2.214
M(III)---O	2.323-2.793[d]				2.77, 3.52, 3.62[k]			
M(III')---O	2.247-3.473[d]							

[a] number of sites

[b] Na(I)---O_3 bond values.

[c] Na(I)---O_2 bond values

[d] M---O bond values are the average bond lengths below 2.500Å and above 2.500Å, respectively. M are metal cation (Na or Cu).

[e] Na(I')---$O_{2\ or3}$ bond values

[f] Na(I'_A)---$O_{2\ or\ 3}$ bond values

[g] Na(II)---$O_{2\ and\ 4}$ bond values

[h] Na(II)---O_2 bond values

[i] Na(II)---O_3 bond values

[j] Na(II)---$O_{2\ and\ 4}$ bond values

[k] Na(III)---$O_{1,2,3}$ respectively are three bond values

Even if the present study does not report an extensive study of all the possible Al positions, different Al positions were considered in the computed zeolite frameworks[59] to account for different possible cation distributions and Al positions in zeolite frameworks. This is the reason why the average computed (Si/Al)-O and M-O bond lengths in the present Tables could be slightly different while the formula of the zeolites are the same (Tables 1, 2, 3, S2 and S4).

Table 2. Geometrical Parameters (Å) of sodium and copper-exchanged FAU X-type zeolite. Geometry optimizations were performed using the PBE for exchange correlation and PAW method.

Method	PBE		Experimental diffraction data			
Label in the study or ref	C	C	60	61	62	63
Si/Al	1	1	1.09	1.18	1.21	1.18
Formula	$Al_{24}Na_{24}O_{96}Si_{24}$	$Al_{24}CuNa_{23}O_{96}Si_{24}$	$Al_{92}Na_{92}O_{384}Si_{100}$	$Al_{88}Na_{88}O_{384}Si_{104}$	~$Al_{87}Na_{87}O_{384}Si_{105}$	$Al_{88.1}Na_{88.1}O_{384}Si_{103.9}$
Occupied M (metal) site positions	I'(8)[a] III'(8)[a] II(8)[a]	I'(8)[a] III'(8)[a] II(8)[a]	I' III', III'' II	I, I′, II, III′ , III''	I',III',II	I, I′, II, III , J
Si-O_1			1.630	1.623	1.619	1.635
Si-O_2			1.643	1.619	1.630	1.603
Si-O_3			1.650	1.618	1.611	1.714
Si-O_4			1.633	1.615	1.630	1.601
Si-O Average	1.643	1.646	1.639	1.619	1.623	1.638
Al-O_1			1.700	1.708	1.709	1.677

Al-O_2			1.713	1.734	1.721	1.734
Al-O_3			1.713	1.738	1.710	1.654
Al-O_4			1.682	1.707	1.719	1.704
Al-O Average	1.759	1.760	1.702	1.722	1.715	1.692
M(I)---O_1				3.824		
M(I)---O_2				3.555		
M(I)---O_3				2.748		2.761
M(I')---O	2.287-2.952*		2.266-2.932**	2.242-2.942**	2.241-2.935**	2.265-2.937**
M(I'')---O				2.36-2.97**		
M(II)---O	2.350-2.898*	2.098-3.096*[i]	2.355-2.885***	2.343-2.887***	2.364-2.906***	2.369-2.923***
M(III')---O	2.312-2.816*		2.44-2.56***	2.41-2.44***	2.58-2.77***	
M(III'')---O			2.33-2.43***	2.45-2.58***		
M(III''')---O				2.22-2.85***		
M(J)---O						1.88-2.56

SJ position is located in the 12-ring window between two supercages[63]

M= Na or Cu

*the two M---O bond values are the average bond lengths below 2.500Å and the bond lengths above 2.500Å, respectively

**the two M---O bond values are the average bond lengths M---O_2 and M---O_3, respectively

***the two M---O bond values are the average bond lengths M---O_2 or M---O_1 and M---O_4

[i] Only M=Cu values were given

Quantum chemical calculations (QM) results clearly show that both the presence of metal exchanged cations (labelled M) and the Al distribution in the framework strongly decrease the symmetry of the fully siliceous framework.[64] As a consequence, the labels of the oxygen atoms in the faujasite structure (O_1, O_2, O_3 and O_4, depicted Figures 1 and 2) are not the most relevant to interpret the ligand properties of the oxygen atoms because they strongly depend on the aluminum vicinity. Thus, the Tables present averaged values of (Si/Al)-O bond lengths without distinction between O_1, O_2, O_3 and O_4 to avoid biased interpretations.

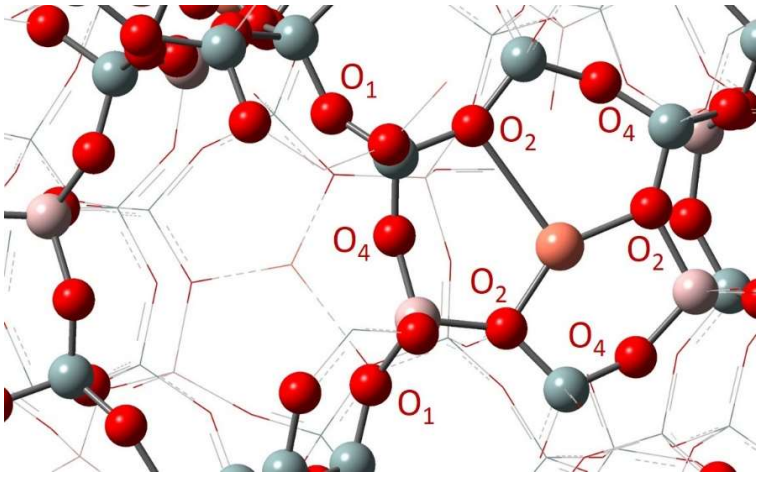

Figure 2. Site II of a Cu^I-exchanged Y-type zeolite (Si/Al larger than 1) calculated using PBE method: Si are grey spheres, O are red spheres, Al are light pink spheres and Cu are brown spheres. In the present model, the copper metal active site at site II is connected to 3 short Cu---O_2 bonds each widely spaced by longer Cu---O_4 bonds. DFT investigations are able to discriminate between short bond lengths and long bond lengths in contrast with XRD analysis.

Moreover, present QM calculations reveal that M---O_4 bond length in six-membered rings (Figure 1, Table S1) can be either smaller or larger than M---O_2 bond length in six-membered rings, which, of course, is not evidenced in averaged bond lengths from X-Ray diffraction results. As reported for copper in Table S1, the coordination number (CN), defined as the number of Cu--

-O bond lengths in site II smaller than the arbitrary value of 2.5 Å, depends on the Si/Al ratio and Al positions in the six-membered ring of sites II.

Present calculated values (Tables 1 and 2) provide information at the molecular scale of the geometry showing that the Si-O bond and Al-O bond distances are not the same. Such results are inaccessible using XRD and most of the spectroscopic methods (mainly EXAFS) provide averaged (Si/Al-O) values depending on the O atoms, being a O_1, O_2, O_3 or a O_4, as a result of symmetry constraints. Despite different methodologies to determine Al atoms distribution[65-66] it is still difficult to determine accurately the Al positions in the zeolite framework.[67]

For Si/Al larger than 1, non-random Al positions in the faujasite are possible[59] with significant changes calculated for the four and six-membered ring symmetries, as previously reported.[64] Thus, average bond distances (Tables 1 and 2) such as those provided from XRD cannot be considered as markers of the structures. This is the reason why present computed average bond distances do not correspond to the average experimental values: for example, XRD measurements provide average values of three (Si/Al)-O_2 bond lengths while QM calculations provide average values of the shortest bonds (smaller than a threshold of 2.5 Å). QM calculations reveal how the aluminum distribution induces the local lack of symmetry of the six- and four-membered rings, whereas this structure disorder could be hard to see within X-Ray diffraction.[68] Focusing on oxygen labels by comparing O_2 vs O_4 leads to an oversimplified scheme of the local structures, in which the role of aluminum distribution is overshadowed.

In addition, experimental bond length values depend on the authors as reported in Tables 1 and 2. In this context, it is difficult to compare QM calculated bond lengths with experimental values. A crude approximation indicates that they are in the same range of values.

A detailed analysis of the coordination of the metal ions shows that it depends on the Al loading and position in the rings, especially for copper (Table S1), as it was previously reported.[64] Because the M---O_{FAU} interaction forces are larger for Cu^{I} than for Na^{I}, the distortion of the rings are larger for Cu^{I} than for Na^{I}.[64]

In the present computational study, no M at site I were found, whatever the Al-distribution in the X- and Y-type faujasite zeolites, while occupation at site I is reported in the literature.[55-56, 58, 60-63, 69] Present calculations show that the Al distribution influence the occupation of site I' but despite large investigations of different structures, no structure with metal cations at site I (M = Na or Cu) was obtained. In addition, in the X-FAU type where the Al distribution is strongly limited in comparison to the large possible Al distributions in the Y-FAU type, no metal cations at site I were located. Such results are in line with the conclusion that most probably synthesis routes play a crucial role in the final structures[70] and suggest that positions such as SJ and SI (Tables 1 and 2) are not frequently occupied if they exist. Even if the experimental metal/aluminum ratio were not provided in the experimental data from Tables 1 and 2, the present conclusions will not change due to a possible low Cu/Al exchange of the zeolite.

Addition of CO on metal-exchanged faujasite structures

As previously mentioned, adsorption of CO is frequently used as probe molecule in FT-IR in situ experiments. According to the literature, only sites located in the largest cages (e.g. sites II and III of the supercages in Figure 1) are accessible to CO.[6]

In the present study, different loadings of CO were calculated (Tables 3, S2-S5) in Y-type FAU zeolites, from 1 CO to 12 CO/primitive unit cell in order to identify the different possible bond types and to analyze the influence of both the Si/Al ratio and Al distribution in six-membered rings. Thus multiple and single adsorptions of CO were considered, including its interaction with

the O atoms, both in a single adsorption (SI) providing a M…O=C structure and a double interaction of CO (DI) providing a M…C=O…M structure originally reported using cluster models.[71]

Table 3. CO adsorption in sodium and copper-exchanged FAU Y-type zeolites unit cells. Comparison of Geometrical Parameters (Å) between DFT calculations and experiments of the addition of one, eight and twelve CO. Two periodic models (labelled A and B) were optimized. Model B with the $C_8Al_{14}Cu_{14}O_{104}Si_{34}$ formula contains one Al-O-Si-O-Al-O-Si-O-Al sequence but not model B with the $C_8Al_{14}Na_{14}O_{104}Si_{34}$ formula.

Method	PBE					**Experimental diffraction and Spectroscopic data[58]**
labelled	A	A	B	A	B	Si/Al=2.7
Formula	$C_1Al_{14}Na_{14}O_{97}Si_{34}$	$C_{12}Al_{14}Na_{14}O_{108}Si_{34}$	$C_8Al_{14}Na_{14}O_{104}Si_{34}$	$C_1Al_{14}CuNa_{13}O_{97}Si_{34}$	$C_8Al_{14}Cu_{14}O_{104}Si_{34}$	$Cu^{I}Y$
Occupied metal site positions (number of sites)	I'(3) III(1) III'(2) II(8)	I'(3) III(1) III'(2) II(8)	I'(6) II(8)	I'(3) III(2) III'(1) II(8)	I'(6) II(8)	
(Si/Al)-O Average	1.703	1.706	1.705	1.704	1.684	
M(I')---O*	2.279-3.014	2.290-2.957	2.284-2.949	2.280-3.022	1.9103-2.942	

					1.8921-2.9436
M(II)---O*	2.355-2.846	2.359-2.829	2.393-2.822	2.359-2.946	
M(III)---O*	2.319-2.799	2.347-2.999		2.293-2.882	
M(III')---O*	2.248-3.479	2.304-3.237		2.367-2.893	

*the two M---O bond values are the average bond lengths below 2.500Å and the bond lengths above 2.500Å, respectively

The adsorption of CO may change the copper cation location. A first indicator is the "Cu displacement", defined as the distance between the copper at site II and any plane containing three O atoms centered toward the six-membered ring, before and after CO adsorption. As previously reported for small cluster models and for a periodic primitive unit cell, the Cu displacement may reach a value of 1 Å.[20, 71] Such a displacement fits with the experimental value of 0.975 Å.[58] In contrast, no significant displacement was calculated for Na^{I} (0.4 Å).[20, 71] Simultaneously, the metal coordination number (CN) may also change within the formation of a short bond distance between the metal and the carbon atom of the carbonyl. To achieve this coordination for copper, the metal CN with the oxygen atoms of the zeolite framework may change (Tables S1 and S3). Finally, the position of the copper metal cation in the ring may have changed significantly upon addition of CO to a position out of the plane of the ring by 0.9 Å.[71] This "rearrangement" is either very large or small, exhibiting significant or small changes of the Cu…O bond distances, as shown in Tables S2 and S3 on the example of the adsorption of 8 CO on 8 Cu^{I} at site II in Y-type FAU $(CO)_8Cu_8Al_{14}O_{98}Si_{34}$.

As shown in Table S2, the adsorption of CO may shift the sodium cations from their original positions even if the changes are less important than for copper.[71] The present study shows that addition of several CO molecules may cause a displacement of metal cations from their original position as it was previously mentioned for the addition of one CO molecule.[20] According to the present calculations, while the two geometry optimizations of $(OC)_{12}Al_{14}Na_{14}O_{96}Si_{34}$ using PBE and PAW method (Table S2) and PBE-D*/BS1 method lead to the same structure with 3 SI', the optimization using the B3LYP-D*/BS1 method converged to Na^{I} metal cation at site I: this is a unique situation where sites I were calculated to be occupied by cations.

This $(OC)_{12}Al_{14}Na_{14}O_{96}Si_{34}$ model was built to investigate different configurations of coordination in a unique unit cell. Different CO positions were considered in such a large model showing that CO polyadsorption provides geometries containing two or three CO molecules adsorbed on one metal site that are minima on the Potential Energy Surface. The geometry optimizations also evidenced dual CO adsorption (e.g. involving two metal cations such as M---C=O---M) and O adsorption of CO on Na, similar to those calculated using cluster models, as well as M---O=C geometries.[22] In the unit cell containing 12 CO molecules, the model is not representative of a progressive adsorption coverage process of CO following an established adsorption model such as a type I isotherm model. However, this model indicates that the calculated structure depends on the calculation method with the example of Na^I moving from site I using B3LYP-D*/BS1 to site I' using the PBE-D*/BS1 methods for the $(CO)_{12}Al_{14}Na_{14}O_{96}Si_{34}$ model labelled A. In addition, this model with the $(CO)_{12}Al_{14}Na_{14}O_{96}Si_{34}$ formula reveals that a dual adsorption site is calculated even when 12 CO are loaded in the unit cell. Calculated bond lengths also have different values depending on PBE –D*/BS1 or B3LYP-D*/BS1. Even if a definitive conclusion about a preferential cation position at site I' over site I cannot be drawn, present results suggest that the Potential Energy Surface is most probably relatively flat regarding metal cation positions in the prism cage with a preference for Na^I at site I'. The possible structures without CO were investigated using PBE, confirming a large preference for NaY type structures with Na at sites I' (Table 1).

Whatever the calculation method, as expected, M cations are connected to O from proximate Al tetraedra. Such tendency remains the same after CO adsorption. Regarding the CN of copper (Tables S1 and S3), it may change after CO addition from 2 or 3 to 3. The coordination with the carbonyl ligand is favoured and in the adsorption process, the copper cation may lose bonds with

the zeolite framework: the number of Cu---O_{FAU} bonds is calculated to become smaller after CO addition (from 2 or 3 to 2).

As the coordination sphere of the metal cation may reorganize upon CO adsorption, it could question the use of CO as a probe of the metal environment. As CO is a popular probe-molecule for *in-situ* infrared spectroscopy, we studied how the local structure of the metal exchange site influences the IR ν_{CO} stretching frequency of CO adsorbed on metal cations (Na^I or Cu^I). We considered a model containing 8 CO molecules, with identical coverage on each metal cation in the supercage, providing the $(OC)_8M_{14}Al_{14}O_{96}Si_{34}$ formula (M= Na or Cu). We compared the ν_{CO} stretching signal for zeolites exchanged with Na^I vs Cu^I and looked for trends depending on the aluminum content of the 6MR involved in the CO adsorption.

The ν_{CO} frequencies calculated in periodic conditions with PBE (Figure 3) show that, when CO adsorbs on metal cations, the ν_{CO} signal is shifted in comparison with free CO in gas phase: at higher frequencies for Na^I-exchanged faujasite, and at both higher and lower frequencies for Cu^I-exchanged faujasite. Moreover, the ν_{CO} massif calculated with Na^I-exchanged faujasite did not overlap with the one of Cu^I-exchanged faujasite. Those results (shift directions, no overlapping) are consistent with the experimental observations (2143 cm^{-1} for gas phase CO, 2165 and 2176 cm^{-1} for CO on Na^I-exchanged X faujasite,[72], 2160, 2145, 2138 and 2128 cm^{-1} for CO on Cu^I-exchanged Y faujasite[73]). From a method point of view, the same trends were obtained with B3LYP functional (Figure S1 and Table S5) but the frequency values (including the gas phase one) are upshifted from PBE to B3LYP by approximatively 100 cm^{-1}. A similar upshift from PBE to B3LYP was previously calculated using cluster models, whatever the metal cation, being copper[74] or sodium.[22]

Beyond the values of the ν_{CO} shifts (Figure 3 and Table S5), the distribution of Na sites causes a spreading of the calculated ν_{CO} frequency values in a range of only 13 cm^{-1} for the 8 CO of the $(OC)_8Na_{14}Al_{14}O_{96}Si_{34}$ model (labelled B). On Cu sites, the results obtained with the analogous model $(OC)_8Cu_{14}Al_{14}O_{96}Si_{34}$ (labelled B) show that the calculated frequency range is larger for Cu (~45 cm^{-1}) than for Na (~13 cm^{-1}). This result suggests that the spectral massif associated with the ν_{CO} signal would be much larger for CO adsorbed in Cu-exchanged Y-type FAU than in Na-exchanged Y-type FAU. This difference in the massif width can be discussed in the light of experimental results, keeping in mind some hypotheses.[5, 72-73] Indeed, the experimental ν_{CO} massif width depends on the intrinsic frequencies of each possible CO adsorbed species (as calculated in the present study) but also on the effective coverage of the adsorption sites in the experimental conditions. As the adsorption of CO is much less exothermic on Na^I sites (~-25 $kJ.mol^{-1}$)[5] than on Cu^I sites (~-80 $kJ.mol^{-1}$),[73] the phenomenon is not characterized under the same conditions for Na-exchanged (under 213 K) and Cu-exchanged faujasites (at room temperature). With those reservations on the effective coverage, we can compare the spreading of the frequencies in the ν_{CO} massif, evaluated from the difference between the highest and the lowest frequencies picked by the authors. It appears in the experimental literature that this numerical spreading is lower for Na-exchanged faujasites (11 cm^{-1} in X faujasite below 213 K)[72] than for Cu-exchanged faujasites (32 cm^{-1} in Y faujasite at room temperature),[73] consistently with the suggestion from the present calculations.

The band broadenings are associated with different Si/Al ratio in the 6 MR. In the Na-exchanged model $(OC)_8Na_{14}Al_{14}O_{96}Si_{34}$ (labelled B), the most upshifted values were calculated for the 6 MR containing only one Al, while the least upshifted values were calculated for the 6 MR containing 2 Al atoms. Similarly, in the Cu-exchanged model $(OC)_8Cu_{14}Al_{14}O_{96}Si_{34}$ (labelled B), the increase

of Al in the 6 MR induces a downshift of the ν_{CO} value. This result combined with previous calculations clearly showed that the frequency values were sensitive to the proximity of Al atoms in the rings e.g. the Si/Al ratio from the 6 MR (leading to a downshift calculated for Al-rich 6 MR), as it was previously shown.[20, 71, 75] Present results suggest that the bandwidth of the ν_{CO} stretching mode is a marker of the Al distribution in the 6 MR of the zeolite (Figure 3, Figure S1 and Table S5). In the case of Cu-exchanged FAU, this influence of the Al distribution is particularly visible in the calculated data set. Experimentally, for the largest ν_{CO} downshifts, we may assume that this Al distribution factor cumulates with another downshift factor not studied here: the possibility for CO to create a double interaction with two exchanged cations. Indeed, in the case of (Na,Cu)-faujasites, previous calculations have shown that the formation of a double interaction (DI) Cu^{I}---C=O---Na^{I} could also cause a downshift of the ν_{CO} in comparison with the gas phase, as observed experimentally at around 2140 cm^{-1}.[20, 22, 71]

The extent and the direction of the ν_{CO} shift relate to the Al distribution, the possibility of double interaction but also to the nature of the exchanged metal and of the interactions it creates with CO and the zeolite framework. In the model containing Cu instead of Na, the ν_{CO} frequency values calculated using the PBE method clearly downshifted and did not overlap, while the C=O bond lengths increased (Figure 3). As indicated above, the calculated values downshifted for copper in comparison to sodium because of the transition metal character of copper.[18, 76] Cu^{I} interacts strongly with CO in comparison with Na^{I}. The Cu^{I} interaction with CO would result from a synergistic contribution of the σ- and π- bond.[5] A significant π back-bonding from Cu to CO is in line with IR stretching frequency values lower than the one of isolated CO but it does not explain the experimental intense frequency band higher than the one of isolated CO. The ν_{CO} upshift reveals the electrostatic character of M, the influence of which appearing stronger for Na than for

Cu. In the following part, we dissect out contributions to binding interaction and specificity by analyzing an easy-to-use cluster model with different calculation methods.

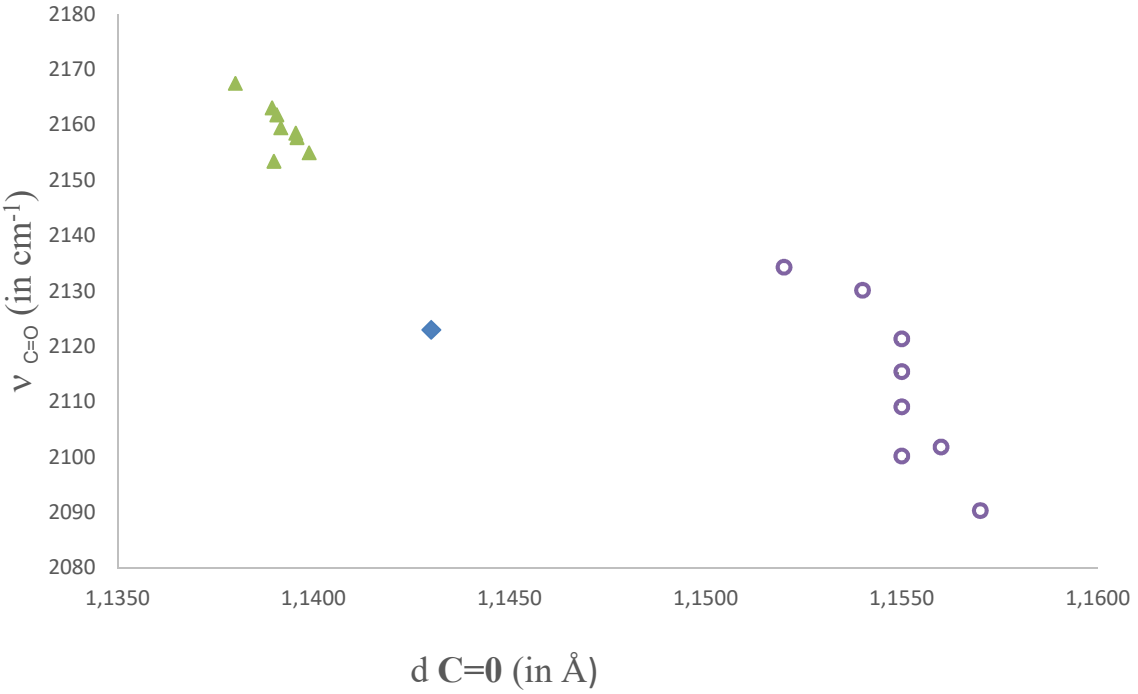

Figure 3. CO in faujasite Y exchanged with Na^I or Cu^I: $\nu_{C=O}$ stretching frequency (in cm^{-1}) as a function of the C=O distance (in Å) calculated with PBE/PAW method in $(CO)_8Na_8Al_{14}O_{98}Si_{34}$ (triangles), $(CO)_8Cu_8Al_{14}O_{98}Si_{34}$ (circles) and CO_{gas} (diamond, modeled in a periodic box).

In previous studies, it was concluded that Na^I behaves like an electrostatic acid and Cu^I like a covalent acid.[12] Recent developments in computational chemistry methods allow to investigate, analyze and characterize the nature of Lewis acids such as Na^I and Cu^I interacting with the faujasite zeolite and/or with CO. Metal cations at site II (Figure 2) without and with CO were considered.

Without adsorbed CO, the Na^I and Cu^I cations both interact with the oxygen atoms of the 6 MR in a mainly electrostatic manner. In the case of Na^I, three Na---O bonds were evidenced with NBO,

QTAIM and ELF methods (detailed in S1., Figure 4a and Table S6 in Supporting Information) and they were characterized with descriptors consistent with a purely ionic bonding (e.g. natural charge of 0.919). In the case of Cu^{I}, two pairs of Cu---O bonds were distinguished: the two longer bonds were analysed with descriptors typical for van der Waals interactions whereas the two shorter exhibited descriptors consistent with an ionic and weakly covalent bonding (see Figure 4a for the QTAIM result on 6T model). As expected with Cu^{I}, the two latter stronger interactions were directed on both sides of the cation, resulting in an apparent 2-coordinate linear complex. The partial covalent character was evidenced with a natural charge lower for Cu^{I} (0.859) than for Na^{I} (0.919) but the bonding between Cu^{I} and the oxygen atoms remained mainly ionic (detailed in S1.). For both metal cations, the NBO, QTAIM and ELF analyses did not show any basin of electron sharing between the cations and the framework oxygen atoms.

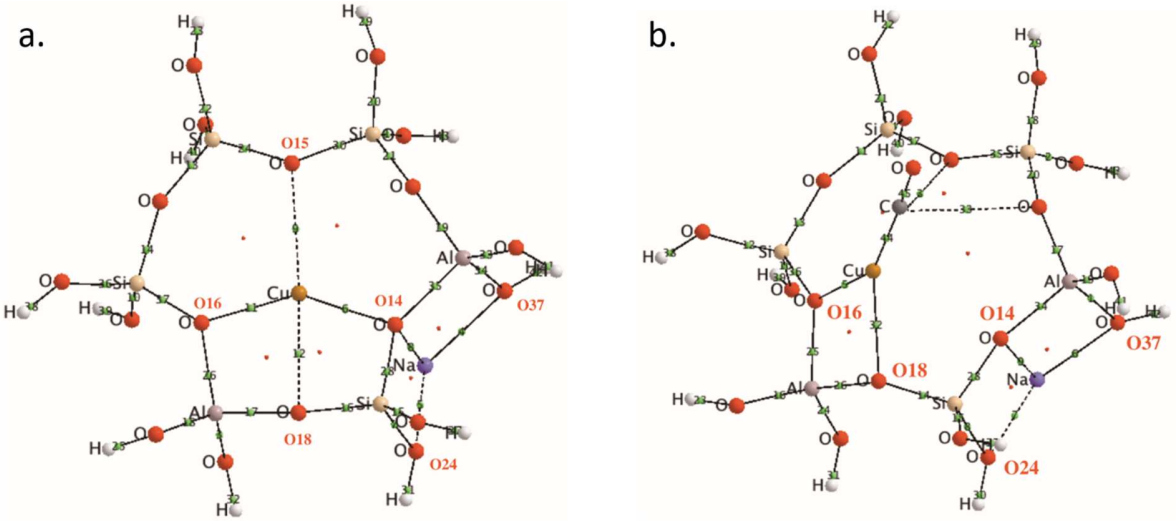

Figure 4. Faujasite Y exchanged with Na^{I} and Cu^{I} without CO (a.) and with adsorbed CO (b.): geometries and QTAIM molecular graphs calculated at the B3LYP/6-311G(d,p) level for the 6T cluster model containing one sodium and one copper metal cations. Red balls are O, white balls are H, brown ball is Cu^{I}, purple ball is Na^{I}, clear skin color balls are Si, pink balls are Al. Bond

critical points (BCPs) are located as small labelled green spheres. See main text and Table S6 for the definition and values of BCP descriptors.

With CO adsorbed on the exchanged metal cation, Na^I and Cu^I behaviors differ more strongly. CO adsorbs on both cations by its C atom but the molecule-cation interaction is electrostatic with Na^I whereas it is a dative σ bond with Cu^I. According to the topological analysis (detailed in S2.), when CO adsorbs on Na^I in the fully Na^I-exchanged zeolite model (Figure 5 and Table S10), the Na^I cation of the adsorption site interacts with the CO molecule and the framework oxygen atoms with purely ionic descriptors. When CO adsorbs on Cu^I in the zeolite model with Cu^I in SII position (Figure 4b, Tables S7 and S8), this Cu^I cation interacts in a different way with CO and the framework oxygen atoms. The Cu^I---CO interaction is characterized with QTAIM and ELF descriptors of a covalent single bond whereas the Cu^I---O_{FAU} interactions remain ionic weakly covalent, as without CO adsorbate.

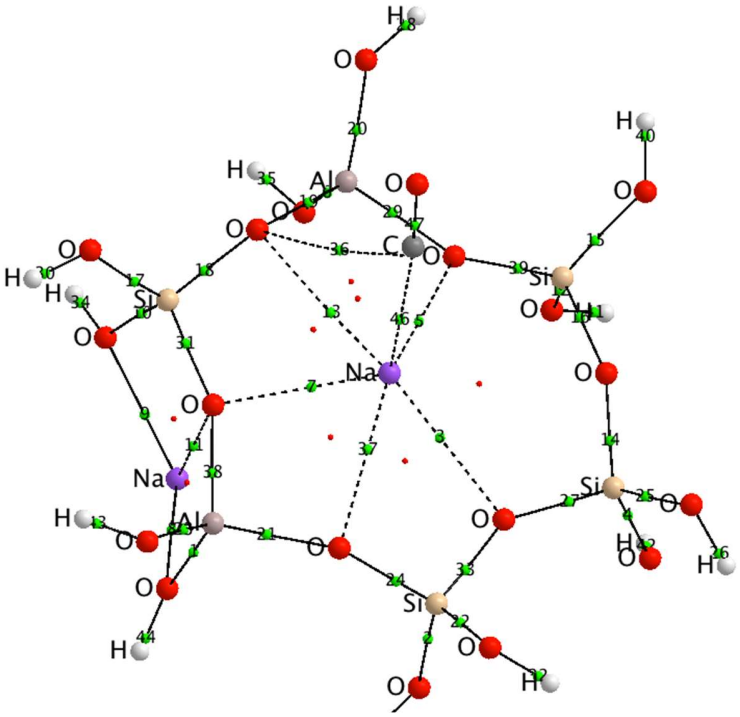

Figure 5. CO adsorbed on faujasite Y exchanged with Na^{I}: geometries and QTAIM molecular graphs calculated at the B3LYP/6-311G(d,p) level for the 6T cluster model containing two sodium cations. Red balls are O, white balls are H, purple ball is Na^{I}, clear skin color balls are Si, pink balls are Al. Bond critical points (BCPs) are located as small labelled green spheres. See main text and Table S7 for the definition and values of BCP descriptors.

The QTAIM charges calculated here for Na^{I} and Cu^{I} in faujasite (resp. 0.90 and 0.75) are in the same range as values previously calculated in chabazite zeolite.[74] In the latter study, the QTAIM atomic charges were calculated for extra-framework Cu^{I} or Cu^{II} cations (0.76-0.80 and 1.29-1.32 respectively), using hybrid DFT (PBE0, HSE03 or HSE06).[74] The QTAIM charge for extra-framework Cu^{I} was thus consistently calculated between 0.75 and 0.80 in faujasite and chabazite zeolites with hybrid DFT. In chabazite, the QTAIM atomic charges of extra-framework Cu^{I} or Cu^{II} cations were reported to be almost unchanged upon adsorption of CO.[74] The same holds for the faujasites of this work, for which QTAIM atomic charges are calculated at 0.83 for Cu^{I} and 1.22 for Cu^{II} upon CO adsorption.

Interestingly, the QTAIM analysis evidences that the Cu^{I} interactions with the zeolite framework oxygen atoms (Figure 4a) reorganize upon CO adsorption: from an apparent 2-coordinate linear complex stabilized with 2 van der Waals interactions without adsorbate, the Cu^{I} coordination changed into a distorted trigonal planar geometry, with two 6 MR geminal oxygen atoms on one side and the CO ligand on the other (Figure 4b).

To complete our topological analysis of the copper cation interacting with zeolites, we extended our perspective by studying the behavior of faujasite exchanged with Cu^{II} in SII exchange position, at the centre of the 6 MR (Figure S4 and Table S9). The results (detailed in S3.) showed that the

bonds between the copper cation and the zeolite framework oxygen atoms have a higher covalent character for Cu^{II} than for Cu^{I}. Inversely, the Cu^{II}---CO bond seems to be less covalent than the Cu^{I}---CO bond. Concerning the nature of their Lewis acidity in zeolite environment, both Cu^{I} and Cu^{II} appeared very versatile and no general conclusion can be drawn without precision of the Lewis base involved in their interactions.

Present calculations revealed that Na^{I} Lewis acid belongs to electrostatic acid family as well as the Cu^{I} Lewis acid when Cu^{I} interacts with zeolite framework oxygen ligands, in contrast with previous conclusions.[12] More precisely, present studies clearly indicated that the Lewis acid properties depend on the atom types in interaction: coordination of carbon monoxide CO through the C atom results in an electrostatic interaction with Na^{I} and a dative bond with a strong covalence degree with Cu^{I}. In contrast, Cu^{II} Lewis acid exhibited both electrostatic and covalent contribution as suggested by the weakening of the dative Cu^{II}-CO bond and the CN increasing from two to three (detailed in S3.). The present analyses (NBO, QTAIM and ELF) converged to the same conclusions regarding the electrostatic nature of the interaction of Na^{I} and Cu^{I} with the O atoms of the FAU zeolite whatever the models 6 T and 43 T were used.

Finally, the topological analysis of the metal cation---CO interactions allow us to explain the shift of the ν_{CO} stretching band value of CO adsorbed on Na^{I} and on Cu^{I} in faujasite zeolites. When an electrostatic interaction occurs between CO and the metal cation such as Na^{I}, the ν_{CO} band is upshifted in comparison with isolated CO. When comparing between the interaction of CO and the metal such as Cu^{I} in which the interaction has a higher covalent character, the ν_{CO} band is less upshifted in comparison with isolated CO and less upshifted than the one of CO adsorbed on Na^{I}-exchanged faujasite. Indeed, the Cu^{I}---CO dative bond was calculated to be highly polarized (detailed in S2.). Such behaviour revealed that even with a soft CO ligand, the Cu^{I}---CO interaction

keeps an ionic character. Present analyses explained why the ν_{CO} stretching band value depended on the configuration of the exchange site and was slightly upshifted in comparison with the ν_{CO} stretching band value of CO in gas phase.

Conclusions

The present DFT study revealed the microscopic structure of metal sites of faujasite zeolites that were not accessible experimentally, depending on the Si/Al ratio and on the nature of the metal cation. It showed that the alkali and transition metal ion exchanged were not necessarily connected to 3 short bonds each widely spaced by longer bonds. In addition, DFT investigations are able to discriminate between short and long bond lengths. Present results showed a decrease of the symmetry of the crystallographic sites in comparison with those generally considered for zeolites. In addition, this quantum chemistry investigation showed that there were no cation at site I. The same tendencies were predicted in faujasite with Si/Al ratio of 1.

The number of Al in the 6 membered ring was clearly reflected in the calculated ν_{CO} vibrational frequency values in the Y-type faujasites and the frequency distribution is larger for CO adsorbed on Cu^I than on Na^I. The calculated values were downshifted by approximatively 100 cm^{-1} from B3LYP to PBE methods.

Present results showed that the electrostatic character of M (Cu^I or Na^I) was revealed in the ν_{CO} stretching band values that were clearly upshifted for Na^I in comparison with Cu^I. While QM correlation between ν_{CO} vibrational frequency values and the C=O bond distance was expected, topological analyses were used to provide more information about the nature of the chemical interaction between metal cations and adsorbed CO. Topological analyses clearly indicated that whatever the metal alkali or transition metal ion, the nature of the interaction with the zeolite

framework is mainly ionic. Even if in the case of Cu^I, a dative Cu---CO bond was evidenced after addition of CO at copper site, it kept an ionic character. These analyses supplement ν_{CO} vibrational frequency values and characterized M---O_{FAU} and M---CO interactions.

Acknowledgment.

This work was performed using HPC resources from GENCI-[CCRT/CINES/IDRIS] (Grants No. 2010-x2011081071, A0010807394 and A0050807394).

Supporting Information.

Geometry parameters calculated using PBE and PAW methods and experimental data are in Tables S1-S4, calculated frequency values are given in Table S5 and in Figure S1. Calculated QTAIM descriptors of zeolite cluster models in Figures S2-S5 are given in Tables S5-S6-S7-S8-S10, calculated ELF descriptors of zeolite cluster model in Figure S4 are given in Table S9, and topological analyses used to characterize Cu^I and Na^I interactions are detailed in paragraphs S1, S2 and S3.

References.

1. Van Speybroeck, V.; Hemelsoet, K.; Joos, L.; Waroquier, M.; Bell, R. G.; Catlow, C. R. A., Advances in theory and their application within the field of zeolite chemistry. *Chem. Soc. Rev.* **2015,** *44* (20), 7044-7111.
2. Li, Y.; Yu, J., New Stories of Zeolite Structures: Their Descriptions, Determinations, Predictions, and Evaluations. *Chem. Rev.* **2014,** *114* (14), 7268-7316.
3. Berthomieu, D.; Delahay, G., Recent advances in CuI/IIY: experiments and modeling. *Catal. Rev. - Sci. Eng.* **2006,** *48* (3), 269-313.
4. Smith, J. V., Faujasite-type structures. Aluminosilicate framework. Positions of cations and molecules. Nomenclature. *Advan. Chem. Ser.* **1971,** *101*, 171-20.
5. Hadjiivanov, K. I.; Vayssilov, G. N., Characterization of oxide surfaces and zeolites by carbon monoxide as an IR probe molecule. *Adv. Catal.* **2002,** *47*, 307-511.

6. Huber, S.; Knozinger, H., Adsorption of CO on sodium containing X- and Y-zeolites and determination of the aluminum distribution. *Appl. Catal., A* **1999,** *181* (2), 239-244.
7. Glendening, E. D.; Landis, C. R.; Weinhold, F., Natural bond orbital methods. *Wiley Interdiscip. Rev.: Comput. Mol. Sci.* **2012,** *2* (1), 1-43.
8. Lepetit, C.; Fau, P.; Fajerwerg, K.; Kahn, M. L.; Silvi, B., Topological analysis of the metal-metal bond: A tutorial review. *Coord. Chem. Rev.* **2017,** *345*, 150-181.
9. Massiani, P.; Fajula, F.; Figueras, F.; Sanz, J., Silicon-29 and aluminum-27 MAS NMR study of the distribution of silicon and aluminum atoms in various forms of synthetic zeolite omega. *Zeolites* **1988,** *8* (4), 332-7.
10. Sklenak, S.; Dedecek, J.; Li, C.; Wichterlova, B.; Gabova, V.; Sierka, M.; Sauer, J., Aluminum siting in silicon-rich zeolite frameworks: a combined high-resolution 27Al NMR spectroscopy and quantum mechanics/molecular mechanics study of ZSM-5. *Angew. Chem., Int. Ed.* **2007,** *46* (38), 7286-7289.
11. Fyfe, C. A.; Gobbi, G. C.; Kennedy, G. J.; Graham, J. D.; Ozubko, R. S.; Murphy, W. J.; Bothner-By, A.; Dadok, J.; Chesnick, A. S., Detailed interpretation of the silicon-29 and aluminum-27 high-field MAS n.m.r. spectra of zeolites offretite and omega. *Zeolites* **1985,** *5* (3), 179-83.
12. Zhang, Y., Electronegativities of elements in valence states and their applications. 1. Electronegativities of elements in valence states. *Inorg. Chem.* **1982,** *21* (11), 3886-9.
13. Reed, A. E.; Weinhold, F., Natural bond orbital analysis of near-Hartree-Fock water dimer. *J. Chem. Phys.* **1983,** *78* (6, Pt. 2), 4066-73.
14. Bader, R. F. W., *Atoms in molecules*. Clarendon Press: Oxford, 1990.
15. Silvi, B.; Savin, A., Classification of chemical bonds based on topological analysis of electron localization functions. *Nature* **1994,** *371* (6499), 683-6.
16. Berthomieu, D.; Krishnamurty, S., Characterization of Structure and Reactivity of Transition Metal Ions in Zeolites Using Static and Molecular Dynamics DFT Calculations. In *Quantum Chemical Calculations of Surfaces and Interfaces of Materials* Ugliengo, V. A. B. a. P., Ed. Stevenson Ranch, CA 91381, USA, 2009; pp 107-132.
17. Klaeui, W.; Lenders, B.; Hessner, B.; Evertz, K., Preparation and characterization of copper(I) complexes with unsaturated small molecules. Crystal structure determination of a copper carbonyl complex stabilized by a tris-chelating oxygen ligand. *Organometallics* **1988,** *7* (6), 1357-63.
18. Pike, R. D., Structure and Bonding in Copper(I) Carbonyl and Cyanide Complexes. *Organometallics* **2012,** *31* (22), 7647-7660.
19. Smith, J. V., Topochemistry of zeolites and related materials. 1. Topology and geometry. *Chem. Rev.* **1988,** *88* (1), 149-82.
20. Nour, Z.; Petitjean, H.; Berthomieu, D., Cooperative Cation Migrations upon CO Addition in CuI- and Alkali-Exchanged Faujasite: A DFT Study. *J. Phys. Chem. C* **2010,** *114* (41), 17802-17811.
21. Loewenstein, W., *Am. Mineral.* **1954,** *39*, 92.
22. Nour, Z.; Berthomieu, D., Multiple adsorption of CO on Na-exchanged Y faujasite: a DFT investigation. *Mol. Simul.* **2014,** *40* (1-3), 33-44.
23. Becke, A. D., A new mixing of Hartree-Fock and local-density-functional theories. *J. Chem. Phys.* **1993,** *98* (2), 1372-7.

24. Lee, C.; Yang, W.; Parr, R. G., Development of the Colle-Salvetti correlation-energy formula into a functional of the electron density. *Phys. Rev. B: Condens. Matter* **1988,** *37* (2), 785-9.
25. Perdew, J. P.; Burke, K.; Ernzerhof, M., Generalized gradient approximation made simple. [Erratum to document cited in CA126:51093]. *Phys. Rev. Lett.* **1997,** *78* (7), 1396.
26. Perdew, J. P.; Burke, K.; Wang, Y., Generalized gradient approximation for the exchange-correlation hole of a many-electron system. *Phys. Rev. B: Condens. Matter* **1996,** *54* (23), 16533-16539.
27. Becke, A. D., Density-functional exchange-energy approximation with correct asymptotic behavior. *Phys. Rev. A: Gen. Phys.* **1988,** *38* (6), 3098-100.
28. Civalleri, B.; Zicovich-Wilson, C. M.; Valenzano, L.; Ugliengo, P., B3LYP augmented with an empirical dispersion term (B3LYP-D*) as applied to molecular crystals. *CrystEngComm* **2008,** *10* (4), 405-410.
29. Bloechl, P. E., Projector augmented-wave method. *Phys. Rev. B: Condens. Matter* **1994,** *50* (24), 17953-79.
30. Krieger, J. B.; Chen, J.; Iafrate, G. J.; Savin, A., Construction of an accurate self-interaction-corrected correlation energy functional based on an electron gas with a gap. *Electron Correl. Mater. Prop., 1st, Crete, Greece, June 28-July 3, 1998* **1999**, 463-477.
31. Kresse, G.; Furthmueller, J., Efficient iterative schemes for ab initio total-energy calculations using a plane-wave basis set. *Phys. Rev. B: Condens. Matter* **1996,** *54* (16), 11169-11186.
32. Kresse, G.; Furthmuller, J., Efficiency of ab-initio total energy calculations for metals and semiconductors using a plane-wave basis set. *Comput. Mater. Sci.* **1996,** *6* (1), 15-50.
33. Kresse, G.; Hafner, J., Ab initio molecular dynamics for open-shell transition metals. *Phys. Rev. B: Condens. Matter* **1993,** *48* (17), 13115-18.
34. Kresse, G.; Hafner, J., Ab initio molecular-dynamics simulation of the liquid-metal-amorphous-semiconductor transition in germanium. *Phys. Rev. B: Condens. Matter* **1994,** *49* (20), 14251-69.
35. Dovesi, R.; Orlando, R.; Erba, A.; Zicovich-Wilson, C. M.; Civalleri, B.; Casassa, S.; Maschio, L.; Ferrabone, M.; De La Pierre, M.; D'Arco, P.; Noel, Y.; Causa, M.; Rerat, M.; Kirtman, B., CRYSTAL14: A program for the ab initio investigation of crystalline solids. *Int. J. Quantum Chem.* **2014,** *114* (19), 1287-1317.
36. Catti, M.; Valerio, G.; Dovesi, R.; Causa, M., Quantum-mechanical calculation of the solid-state equilibrium MgO + Î±-Al2O3â†¹MgAl2O4 (spinel) versus pressure. *Phys. Rev. B: Condens. Matter* **1994,** *49* (20), 14179-87.
37. Civalleri, B.; Ugliengo, P., First principles calculations of the adsorption of NH3 on a periodic model of the silica surface. *J. Phys. Chem. B* **2000,** *104* (40), 9491-9499.
38. Peintinger, M. F.; Oliveira, D. V.; Bredow, T., Consistent Gaussian basis sets of Triple-Zeta valence with polarization quality for solid-State Calculations. *J. Comput. Chem.* **2012,** *34* (6), 451-459.
39. Spackman, M. A.; Mitchell, A. S., Basis set choice and basis set superposition error (BSSE) in periodic Hartree-Fock calculations on molecular crystals. *Phys. Chem. Chem. Phys.* **2001,** *3* (8), 1518-1523.
40. Schaefer, A.; Huber, C.; Ahlrichs, R., Fully optimized contracted Gaussian basis sets of triple zeta valence quality for atoms Li to Kr. *J. Chem. Phys.* **1994,** *100* (8), 5829-35.

41. Frisch, M. J.; Trucks, G. W.; Schlegel, H. B.; Scuseria, G. E.; Robb, M. A.; Cheeseman, J. R.; Scalmani, G.; Barone, V.; Mennucci, B.; Petersson et al. *Gaussian09*, Revision D.01; Gaussian, Inc.: Pittsburgh PA, 2009.
42. Schaftenaar, G.; Noordik, J. H., "Molden: a pre- and post-processing program for molecular and electronic structures". *J. Comput.-Aided Mol. Design* **2000,** *14*, 123-124.
43. Ugliengo, P.; Viterbo, D.; Chiari, G., MOLDRAW: Molecular graphics on a personal computer. *Zeitschrift für Kristallographie* **1993,** *207* (part-1), 9-23.
44. Spek, A. L., Structure validation in chemical crystallography. *Acta Cryst.* **2009,** *D65*, 148-155.
45. Glendening, E. D.; Landis, C. R.; Weinhold, F., NBO 6.0: Natural bond orbital analysis program. *J. Comput. Chem.* **2013,** *34* (16), 1429-1437.
46. Glendening, E. D.; Weinhold, F., Natural resonance theory. I. General formalism. *J. Comput. Chem.* **1998,** *19* (6), 593-609.
47. Noury, S.; Krokidis, X.; Fuster, F.; Silvi, B., Computational tools for the electron localization function topological analysis. *Comput. Chem.* **1999,** *23* (6), 597-604.
48. Keith, T. A. *AIMA11*, Version 17.11.14; Overland Park K S, USA, 2016.
49. Bianchi, R.; Gervasio, G.; Marabello, D., Experimental Electron Density Analysis of Mn2(CO)10: Metal-Metal and Metal-Ligand Bond Characterization. *Inorg. Chem.* **2000,** *39* (11), 2360-2366.
50. Macchi, P.; Proserpio, D. M.; Sironi, A., Experimental Electron Density in a Transition Metal Dimer: Metal-Metal and Metal-Ligand Bonds. *J. Am. Chem. Soc.* **1998,** *120* (51), 13429-13435.
51. Espinosa, E.; Alkorta, I.; Elguero, J.; Molins, E., From weak to strong interactions: A comprehensive analysis of the topological and energetic properties of the electron density distribution involving X-H···F-Y systems. *J. Chem. Phys.* **2002,** *117* (12), 5529-5542.
52. Espinosa, E.; Alkorta, I.; Rozas, I.; Elguero, J.; Molins, E., About the evaluation of the local kinetic, potential and total energy densities in closed-shell interactions. *Chem. Phys. Lett.* **2001,** *336* (5,6), 457-461.
53. Espinosa, E.; Molins, E.; Lecomte, C., Hydrogen bond strengths revealed by topological analyses of experimentally observed electron densities. *Chem. Phys. Lett.* **1998,** *285* (3,4), 170-173.
54. Becke, A. D.; Edgecombe, K. E., A simple measure of electron localization in atomic and molecular systems. *J. Chem. Phys.* **1990,** *92* (9), 5397-403.
55. Eulenberger, G. R.; Shoemaker, D. P.; Keil, J. G., Crystal structures of hydrated and dehydrated synthetic zeolites with faujasite aluminosilicate frameworks. I. The dehydrated sodium, potassium, and silver forms. *J. Phys. Chem.* **1967,** *71* (6), 1812-18.
56. Fowkes, A. J.; Ibberson, R. M.; Rosseinsky, M. J., Structural Characterization of the Redox Behavior in Copper-Exchanged Sodium Zeolite Y by High-Resolution Powder Neutron Diffraction. *Chem. Mater.* **2002,** *14* (2), 590-602.
57. Frising, T.; Leflaive, P., Extraframework cation distributions in X and Y faujasite zeolites: A review. *Microporous Mesoporous Mater.* **2008,** *114* (1-3), 27-63.
58. Palomino, G. T.; Bordiga, S.; Zecchina, A.; Marra, G., L.; Lamberti, C., XRD, XAS, and IR Characterization of Copper-Exchanged Y Zeolite. *J. Phys. Chem. B* **2000,** *104*, 8641-8651.
59. Sklenak, S.; Dedecek, J.; Li, C.; Wichterlova, B.; Gabova, V.; Sierka, M.; Sauer, J., Aluminum siting in silicon-rich zeolite frameworks: a combined high-resolution (27)Al NMR

spectroscopy and quantum mechanics / molecular mechanics study of ZSM-5. *Angew Chem Int Ed Engl* **2007,** *46* (38), 7286-9.
60. Zhu, L.; Seff, K., Reinvestigation of the Crystal Structure of Dehydrated Sodium Zeolite X. *J. Phys. Chem. B* **1999,** *103* (44), 9512-9518.
61. Olson, D. H., The crystal structure of dehydrated NaX. *Zeolites* **1995,** *15* (5), 439-43.
62. Vitale, G.; Mellot, C. F.; Bull, L. M.; Cheetham, A. K., Neutron Diffraction and Computational Study of Zeolite NaX: Influence of SIII' Cations on Its Complex with Benzene. *J. Phys. Chem. B* **1997,** *101* (23), 4559-4564.
63. Hunger, J.; Beta, I. A.; Boehlig, H.; Ling, C.; Jobic, H.; Hunger, B., Adsorption Structures of Water in NaX Studied by DRIFT Spectroscopy and Neutron Powder Diffraction. *J. Phys. Chem. B* **2006,** *110* (1), 342-353.
64. Berthomieu, D.; Jardillier, N.; Delahay, G.; Coq, B.; Goursot, A., Experimental and theoretical approaches to the study of TMI-zeolite (TM=Fe, Co, Cu). *Catal. Today* **2005,** *110* (3-4), 294-302.
65. Alberti, A.; Gottardi, G., The determination of the aluminum content in the tetrahedra of framework silicates. *Z. Kristallogr.* **1988,** *184* (1-2), 49-61.
66. Jeffroy, M.; Nieto-Draghi, C.; Boutin, A., New Molecular Simulation Method To Determine Both Aluminum and Cation Location in Cationic Zeolites. *Chem. Mater.* **2017,** *29* (2), 513-523.
67. Sauer, J. In *Zeolite modelling: active sites in different framework structures and in different crystallographic positions*, Royal Society of Chemistry: 2008; pp 441-456.
68. Seo, S. M.; Lim, W. T.; Seff, K. In *Crystallographic verification that copper(II) coordinates to four of the oxygen atoms of zeolite 6-rings: Preparation and two single-crystal structures of fully dehydrated, largely Cu2+-exchanged zeolite Y (FAU, Si/Al = 1.56)*, American Chemical Society: 2013; pp PHYS-301.
69. Fitch, A. N.; Jobic, H.; Renouprez, A., Localization of benzene in sodium-Y-zeolite by powder neutron diffraction. *J. Phys. Chem.* **1986,** *90* (7), 1311-18.
70. Dedecek, J.; Sklenak, S.; Li, C.; Wichterlova, B.; Gabova, V.; Brus, J.; Sierka, M.; Sauer, J., Effect of Al-Si-Al and Al-Si-Si-Al Pairs in the ZSM-5 Zeolite Framework on the 27Al NMR Spectra. A Combined High-Resolution 27Al NMR and DFT/MM Study. *J. Phys. Chem. C* **2009,** *113* (4), 1447-1458.
71. Jardillier, N.; Villagomez Enrique, A.; Delahay, G.; Coq, B.; Berthomieu, D., Probing Cu(I)-exchanged zeolite with CO: DFT modeling and experiment. *J Phys Chem B* **2006,** *110* (33), 16413-21.
72. Busca, G., Acidity and basicity of zeolites: A fundamental approach. *Microporous Mesoporous Mater.* **2017,** *254*, 3-16.
73. Borgard, G. D.; Molvik, S.; Balaraman, P.; Root, T. W.; Dumesic, J. A., Microcalorimetric and Infrared Spectroscopic Studies of CO, C2H4, N2O, and O2 Adsorption on Cu-Y Zeolite. *Langmuir* **1995,** *11* (6), 2065-70.
74. Goeltl, F.; Hafner, J., Structure and properties of metal-exchanged zeolites studied using gradient-corrected and hybrid functionals. III. Energetics and vibrational spectroscopy of adsorbates. *J. Chem. Phys.* **2012,** *136* (6), 064503/1-064503/31.
75. Nachtigall, P.; Frolich, K.; Drobna, H.; Bludsky, O.; Nachtigallova, D.; Bulanek, R., FTIR Study of CO Interactions with Li+ Ions in Micro- and Mesoporous Matrices: Coordination and Localization of Li+ Ions. *J. Phys. Chem. C* **2007,** *111* (30), 11353-11362.

76. Chaquin, P.; Canac, Y.; Lepetit, C.; Zargarian, D.; Chauvin, R., Estimating local bonding/antibonding character of canonical molecular orbitals from their energy derivatives. The case of coordinating lone pair orbitals. *Int. J. Quantum Chem.* **2016,** *116* (17), 1285-1295.